Supplementary Information

All-optical control of high-purity trions in nanoscale waveguide

Hyeongwoo Lee,[1] Yeonjeong Koo,[1] Shailabh Kumar,[2,3] Yunjo Jeong,[4] Dong Gwon Heo,[5] Soo Ho Choi,[6] Huitae Joo,[1] Mingu Kang,[1] Radwanul Hasan Siddique,[2,3] Ki Kang Kim,[6,7] Hong Seok Lee,[5] Sangmin An,[5] Hyuck Choo*,[2,8] and Kyoung-Duck Park*[1]

[1]*Department of Physics, Pohang University of Science and Technology (POSTECH), Pohang 37673, Republic of Korea*

[2]*Department of Medical Engineering, California Institute of Technology (Caltech), CA 91125, USA*

[3]*Meta Vision Lab, Samsung Advanced Institute of Technology (SAIT), CA 91101, USA*

[4]Institute of Advanced Composite Materials, Korea Institute of Science and Technology, Jeonbuk 55324, Republic of Korea

[5]*Department of Physics, Research Institute of Physics and Chemistry, Jeonbuk National University, Jeonju 54896, Republic of Korea*

[6]*Center for Integrated Nanostructure Physics, Institute for Basic Science (IBS), Suwon 16419, Republic of Korea*

[7]*Department of Energy Science, Sungkyunkwan University (SKKU), Suwon 16419, Republic of Korea*

[8]*Advanced Sensor Lab, Device Research Center, Samsung Advanced Institute of Technology (SAIT), Suwon 16678, Republic of Korea*

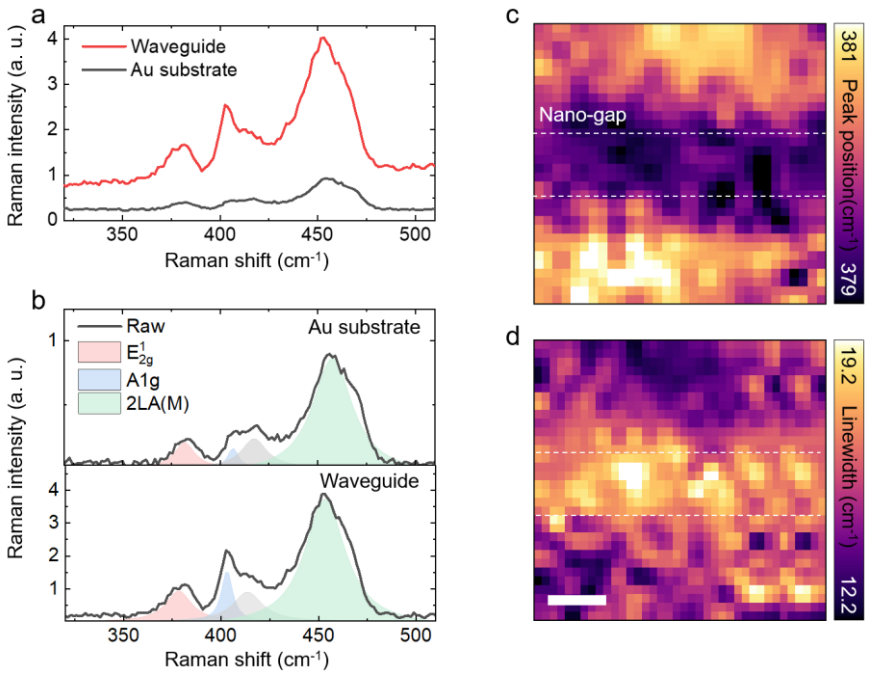

Fig. S1. Raman scattering characteristics of the suspended MoS_2 ML. (a) Raman spectra of MoS_2 ML transferred on Au substrate (black) and suspended on trionic waveguide (red). (b) Lorentz fitted Raman spectra of the MoS_2 ML transferred on Au substrate (top) and suspended on trionic waveguide (bottom). Red, blue, and green filled peaks indicate E^1_{2g}, A_{1g}, and 2LA(M) Raman modes. Peak position image (c) and linewidth image (d) for E^1_{2g} mode Raman spectra. Scale bar is 400 nm.

In order to induce the inhomogeneous strain on the ultrathin trionic waveguide device, the formation of the well-suspended MoS_2 ML on the device is important. We confirm the well-suspended MoS_2 ML by comparing the Raman spectra measured at the Au substrate and the trionic waveguide, as shown in Fig. S1a and S1b [1]. When the MoS_2 ML is suspended, both E^1_{2g} and A_{1g} mode are redshifted with noticeable spectral broadening. Fig. S1c and d show the redshifted peak position with the spectral broadening at the nanogap region, which are in good agreement with the previous studies [2, 3].

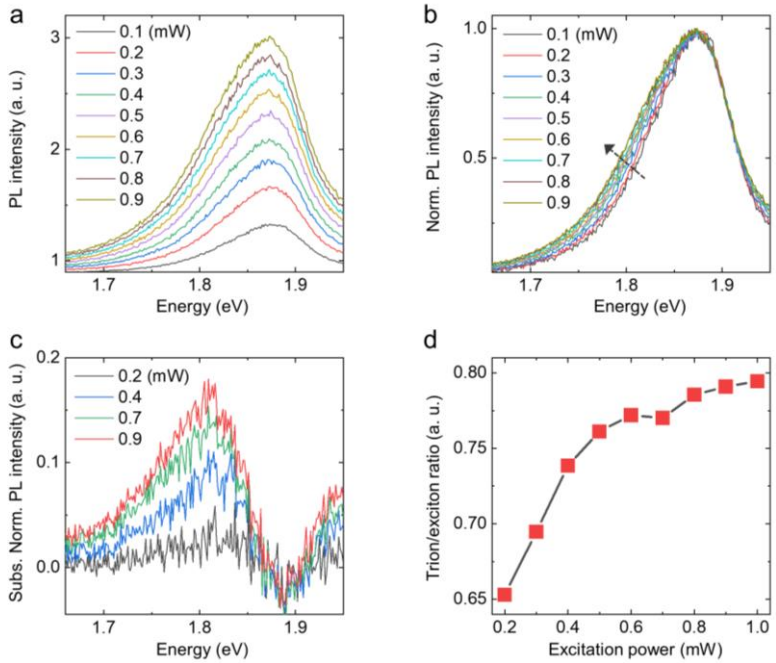

Fig. S2. Power dependence of the incomplete exciton-to-trion conversion. (a) Excitation-power-dependent PL spectra at weak SPP region of trionic waveguide. (b) Normalized PL spectra of (a). (c) Selective subtracted spectra exhibiting pronounced emergence of X- emission. (d) X-/X_0 ratio as function of excitation power.

In order to confirm the deficiency of the electron at the nanogap of the trionic waveguide, which results in the incomplete exciton-to-trio conversion, we gradually measure the PL spectra with increasing excitation power, as shown in Fig. S2a. Even with the relatively high power (~0.9 mW), the trion emission cannot be dominant. Fig. S2b shows the normalized PL spectra. To demonstrate clear spectral change, we show the representative PL spectra after normalization and subtraction by the lowest power PL spectra, as shown in Fig. S2c. The increasing rate of the trion emission becomes low as the excitation power increases, as shown in Fig. S2d. This result is attributed to dominant X_0 density at the nanogap compared to the electron density because the funneling of photoexcited X_0 in the vicinity surpasses the provision of the electrons by the photodoping effect [4, 5].

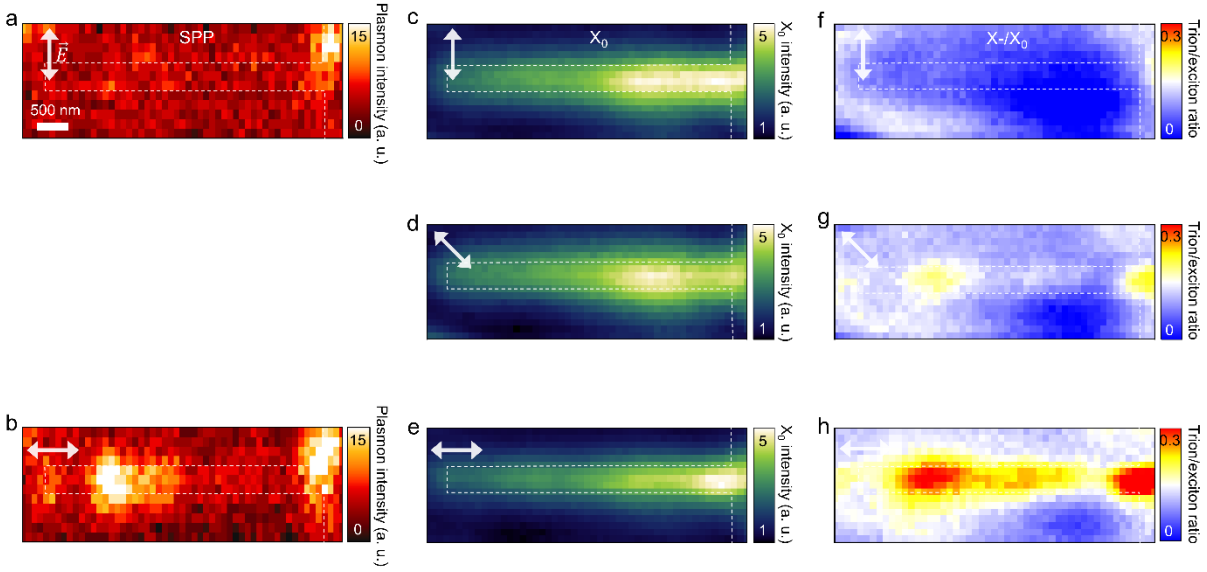

Fig. S3. 2D image of Fig. 2 in the main text. SPP images with excitation polarization across (a) and along (b) waveguide. (c-e) X_0 PL images of with different excitation polarizations. (f-h) PL images of X^-/X_0 ratio with different excitation polarizations. White dashed line is guideline for waveguide structure based on Fig. S4.

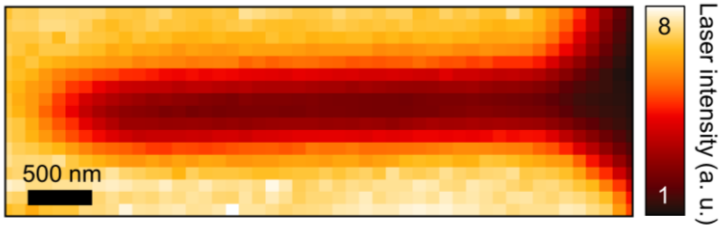

Fig. S4. Rayleigh scattering image of the trionic waveguide. Guideline for scan area in Fig. 2 is based on this Rayleigh scattering image.

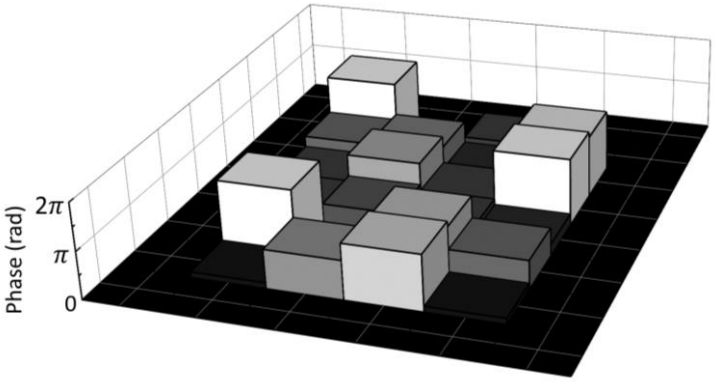

Fig. S5. Optimal phase mask of Fig. 4 in main text.

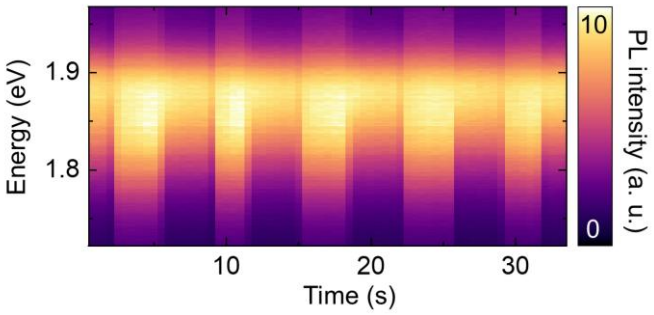

Fig. S6. On/off switching of exciton-to-trion conversion. Time-series PL spectra during on/off switching of exciton-to-trion conversion, before normalization of Fig. 4e.

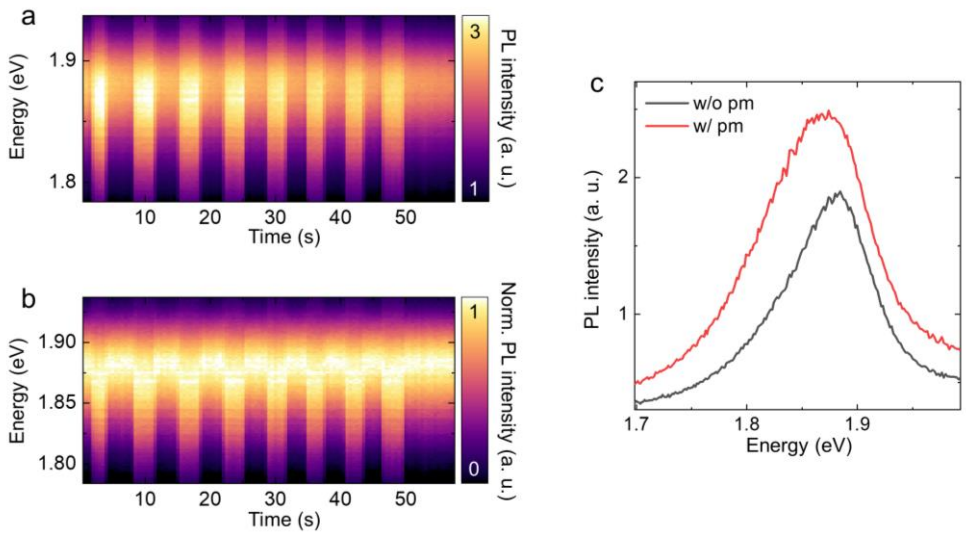

Fig. S7. Reproducibility of modulating exciton-to-trion conversion location. (a) Time-series PL response during on/off switching of exciton-to-trion conversion. (b) Normalization of (a). (c) Representative PL spectra with (red) and without (black) optimal phase mask.

The controllability and reproducibility are confirmed by conducting a wavefront shaping at the different weak SPP region. Fig. S7a shows the dynamic switching between X_0 dominant emission and X- dominant emission with the phase mask optimized for the current location. The normalized spectral image in Fig. S7b and the representative PL spectra in Fig. S7c show the distinct transition between X_0 dominant and X- dominant emissions.

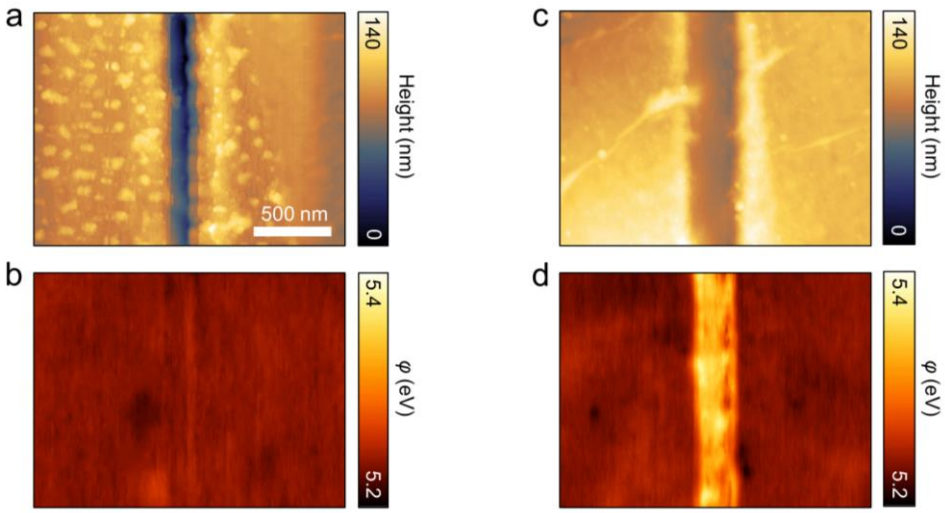

Fig. S8. Work function of MoS_2 ML on nanogap of trionic waveguide. Topography image (a) and corresponding work function image (b) of nanogap without MoS_2 ML. Topography image (c) and corresponding work function image (d) of suspended MoS_2 ML on nanogap.

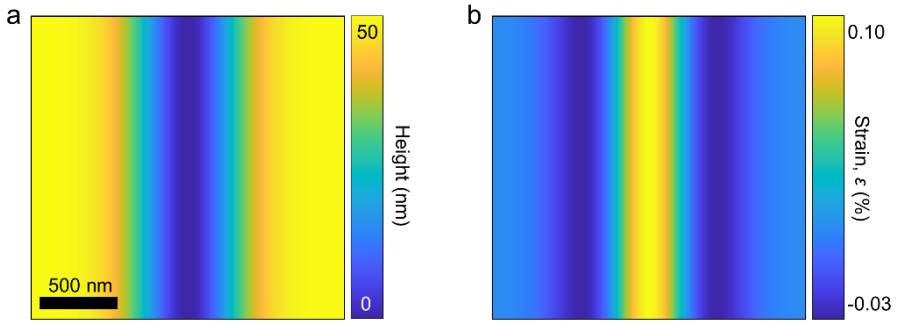

Fig. S9. Estimation of the strain profile. (a) Image of fitted line shape function based on experimentally measured topography profile of MoS_2 ML on nanogap of ultrathin trionic waveguide. (b) Corresponding strain image estimated by continuum theory for a thin and elastic plate [6].

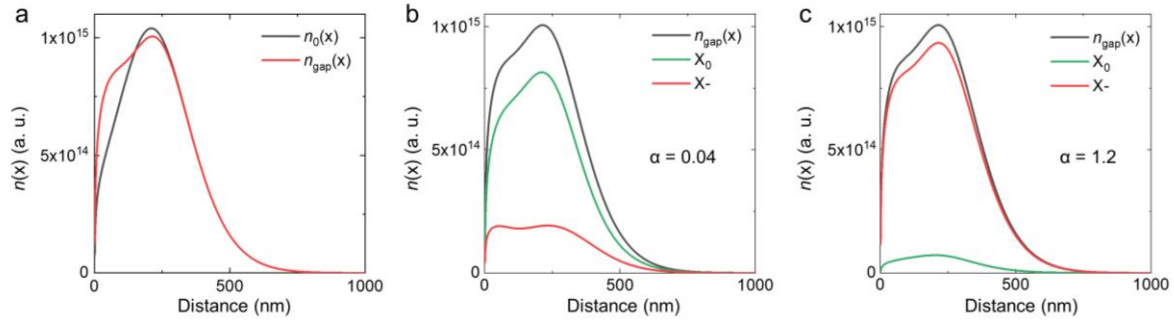

Fig. S10. Estimation of spatial distribution of X_0 and X-. (a) Spatial distribution of the exciton with (red) and without (black) strain gradient. Contribution of X_0 (green) and X- (red) in totally generated exciton density (black) for α = 0.04 (b) and α = 1.2 (c).

As mentioned in the main text, we subtract the exciton density obtained without the strain gradient (black, in Fig. S10a) from the exciton density with the strain gradient (red, in Fig. S10a) to exclude the effect of the optical excitation. At this stage, we exclude the contribution of X- to clearly investigate the exciton movement. Then, we adopt the mass action model to estimate the density ratio of X_0 and X- depending on the background electron density α, as shown in Fig. S10b and S10c.

[1] Fan, J.-H. *et al*. Resonance Raman scattering in bulk 2H-MX_2 (M = Mo, W; X = S, Se) and monolayer MoS_2. *J. Appl. Phys.* **115**, 053527 (2014).

[2] O'Brien, M. *et al.* Raman spectroscopy of suspended MoS_2. *Phys. Status Solidi B* **254**, 1700218 (2017).

[3] Yu, Y. *et al.* Engineering substrate interactions for high luminescence efficiency of transition-metal dichalcogenide monolayers. *Adv. Funct. Mater.* **26**, 4733-4739 (2016).

[4] Currie, M. Hanbicki, A. T. Kioseoglou, G. & Jonker, B. T. Optical control of charged exciton states in tungsten disulfide. *Appl. Phys. Lett*. **106**, 201907 (2015).

[5] Mitioglu, A. A. *et al*. Optical manipulation of the exciton charge state in single-layer tungsten disulfide. *Phys*. Rev. B **88**, 245403 (2013).

[6] Landau, L. D. & Lifshitz, E. *Course of theoretical physics.*